# EMULATION TECHNIQUES FOR SMALL SCALE FADING ASPECTS OF WIRELESS CHANNELS BY USING REVERBERATION CHAMBER
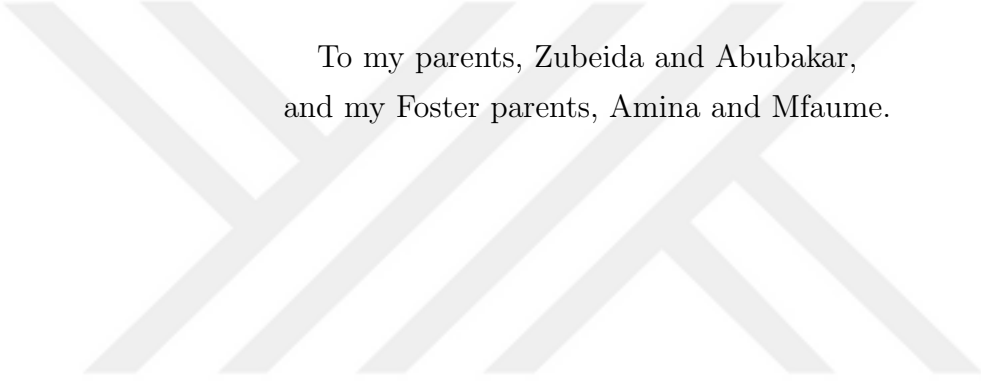
A THESIS SUBMITTED TO

THE GRADUATE SCHOOL OF

ENGINEERING AND NATURAL SCIENCES

OF ISTANBUL MEDIPOL UNIVERSITY

IN PARTIAL FULFILLMENT OF THE REQUIREMENTS FOR

THE DEGREE OF

MASTER OF SCIENCE

IN

ELECTRICAL-ELECTRONICS ENGINEERING AND CYBER SYSTEMS

By

Abuu Bakari Kihero

March, 2018

To my parents, Zubeida and Abubakar,
and my Foster parents, Amina and Mfaume.

# ABSTRACT

# EMULATION TECHNIQUES FOR SMALL SCALE FADING ASPECTS OF WIRELESS CHANNELS BY USING REVERBERATION CHAMBER

Abuu Bakari Kihero

M.S. in Electrical-Electronics Engineering and Cyber Systems

Advisor: Prof. Dr. Hüseyin Arslan

March, 2018

Reverberation chambers (RVCs) are used to provide an effective and reliable testbed for emulating wireless channel effects in the laboratory environment. Various techniques that enrich the capabilities of the RVC in channel emulation have been studied in the literature, however, insufficient control of some of the emulated channel characteristics (like time and frequency dispersions) still leave an open problem for RVC based channel emulators. In this thesis, novel channel emulation techniques by using RVC are introduced to enhance the flexibility in controlling the emulated time and frequency dispersions of the channels. Surface Acoustic Wave (SAW) delay lines and power controllers (i.e amplifiers and attenuators) are used to add degrees of freedom for manipulating the Power Delay Profile (PDP) during delay spread emulation. This technique also overcomes the challenge of achieving higher delay spread values with bench-top sized RVC. The second technique is aimed at enhancing the control of the shape of the Doppler spectrum emulated in the chamber. The proposed techniques are evaluated through mathematical analyses and comparison with the on-site measurement results available in the literature.

*Keywords:* Angle of arrival (AOA), delay spread, channel emulator, Doppler spread, fading statistics, reverberation chamber, surface acoustic wave (SAW) delay lines..

# ÖZET

## KABLOSUZ HABERLEŞME KANALLARIN KÜÇÜK ÖLÇEKLİ SÖNÜMLEME YÖNLERİ İÇİN YANKILAMA ODASI İLE TAKLİT TEKNİKLERİ

Abuu Bakari Kihero

Elektrik-Elektronik Mühendisliği ve Siber Sistemler, Yüksek Lisans

Tez Danışmanı: Prof. Dr. Hüseyin Arslan

Mart, 2018

Yankılama odaları (RVC), laboratuar ortamında kablosuz kanal etkilerini taklit etmek için etkili ve güvenilir bir test yatağı sağlamaya yönelik olarak kullanılmaktadırlar. Kanal taklidi için RVC'nin yeteneklerini zenginleştiren çeşitli teknikler literatürde incelenmiştir. Bununla birlikte, taklit edilen kanal özelliklerinin bazılarının (zaman ve frekansta dağılım gibi) yeterli miktarda kontrol edilemeyisi, yankılama odası tabanlı kanal taklitçileri için çözülememiş bir problem olmaya halen devam etmektedir. Bu tez çalışmasında, taklit edilmiş zaman ve frekans dağılımlarının kontrol edilmesindeki esnekliği arttırmak için yankı odasının kullanıldığı yeni kanal taklit teknikleri önerilmiştir. Yüzeysel ses dalgası (SAW) gecikme hatları ve güç kontrolörleri (yükselteç ve zayıflatıcı), gecikme yayılımı takliti sırasında güç gecikmesi profili (PDP)'yi manipüle etmeye yönelik serbestlik derecesi eklemek için kullanılmıştır. Bu teknik aynı zamanda, küçük boyutlu yankı odası ile daha yüksek gecikme yayılımı değerlerine ulaşma zorluğunu da ortadan kaldırmaktadır. İkinci teknik, yankılama odası içerisinde taklit edilmiş olan Doppler spektrumunun şeklinin kontrolünü arttırmayı amaçlamaktadır. Önerilen teknikler, matematiksel analizler ve literatürde mevcut olan saha ölçüm sonuçları ile karşılaştırılarak değerlendirilmiştir.

*Anahtar sözcükler*: Varış açısı, gecikme yayılımı, kanal taklitçisi, Doppler yayılımı, sönümlenme istatistiği, yankılama odası, Yüzeysel ses dalgası gecikme hatları..

# Acknowledgement

Foremost, I want to offer this endeavor to our God Almighty for the wisdom he has bestowed upon me, the strength, peace of mind and good health in order to finish this research.

I would like to express my sincere gratitude to my advisor, Prof. Dr. Hüseyin Arslan for the continuous support of my Master studies and research, for his patience, motivation, enthusiasm, and immense knowledge. His guidance helped me in all the time of research and writing of this thesis. My sincere thanks also goes to my research mate Mr. Murat Karabacak for his sincere support and contribution throughout the conduction of this research work. Special thanks to my colleagues at CoSiNC research group for the encouragement and advise we share in pursuing and achieving our research goals. Also, I would like to give my kind regards to Mr. Hassan Duman, the secretary of the dean of school of engineering for his close support on the completion of the paperwork of this thesis.

Last but not the least, my heartfelt thanks and appreciation goes to my beloved parents: Zubeida and Abubakar, for giving birth to me at first place and for supporting and shaping me to the individual I am today. May the blessing be showered on them as they have done to me since I was young.

# Contents

# List of Figures

# List of Tables

# Chapter 1

# Introduction

The rapid growth of the wireless technology and its applications leads to the development of new advanced wireless systems and devices. An important development stage for those systems and devices is to evaluate them under realistic channel conditions. However, performing on-site measurements can be a challenging task due to the execution cost, especially for a long range communication system. Channel emulators are known to provide a solution to this challenge by facilitating an efficient and less expensive means of testing wireless systems under realistic channel conditions.

One of the promising wireless channel emulators is a RVC-based emulator. With the help of rotating metallic paddles (stirrer) that constantly randomizes electromagnetic (EM) fields inside the chamber, the RVC can emulate wireless channel effects like frequency and time dispersions [1,2]. A mode stirred RVC with high (above threshold[1]) quality factor[2] (Q-factor) inherently emulates Rayleigh fading statistics of the wireless channel [4]. However, the capability of the RVC can be improved further to emulate other varieties of the wireless channel fading

---

[1]Threshold of the quality factor of RVC is defined as the EM energy level below which further energy loss due to the addition of lossy objects into the chamber is unacceptable and deteriorate the performance of RVC completely. Value of the threshold depends on the size (volume) of the chamber and wavelength of the signal [3].

[2]Q-factor is defined as the ratio of the steady state energy stored within RVC to the dissipated power per RF cycle.

environments, for instance, in [5], an electrically switched multi-element transmitting antenna array is designed to create Ricean and Hyper-Rayleigh fading environment in the RVC. Non-isotropic fading environment inside RVC was also achieved in [6] by controlling the power received from different angles of arrival by using radio frequency (RF) absorbers. The study in [1] analyzes the Doppler spread introduced on the signal due to the continuously rotating stirrer inside RVC whereby different rotational speeds of the stirrer and the existence of RF absorbers are evaluated to generate different bandwidths and shapes of the Doppler spectrum.

In the state of the art, loading RF absorbers into the RVC is the widely used technique for controlling the number of multipath components (MPCs) and delay spread inside RVC [2, 6]. The loaded RF absorbers tend to reduce the ringing down time of the RF signal and so its delay spread. However, the loading technique can only reduce delay spread but not increase it. In case larger delay spread is desired to be emulated, the only option is to use a chamber with relatively larger dimensions. For instance, while the RVC that we have at Istanbul Medipol University has a volume of 0.449 $m^3$ and it can achieve about 50 $ns$ RMS delay spread at 1.25 $GHz$, the NIST (National Institute of Standards and Technology) reverberation chamber used for measurement campaign conducted in [2] has an approximate volume of 38 $m^3$ that achieves about 750 $ns$ RMS delay spread with the same measurement setups. However, building such a big RVCs to achieve more delay spread can be unrealistic in most cases because of the required sizes. Again, the study in [3] points out that loading RVC with RF absorbers has a tendency of reducing the Q-factor of the chamber and deteriorating the spatial uniformity of the EM field. Therefore, in order to maintain the functionality of the RVC, there is always the maximum amount of absorbers that can be loaded into it. Furthermore, it has been shown in [1] that RF absorbing materials alter the distribution of angular spread (AS) in the RVC which directly affects the shape of the Doppler spectrum achieved in the chamber. This leads to the inflexibility in controlling channel characteristics as trying to control delay spread by using the loading technique has a direct impact on angular spread, Doppler spread and EM field distribution within RVC. These existing challenges

2

in emulating wireless channel characteristics by using conventional RVC are the driving force of our study to look for a new approaches that can nurture the ability of the RVC in the wireless channel emulation.

In this thesis, two main channel emulation techniques by using RVC are presented. The first approach targets to control and increase the delay spread of the channel in the chamber by using surface acoustic wave (SAW) delay lines and power controllers. SAW delay lines are used to create channel taps whose delays and powers can be easily adjusted. This makes the control of the delay spread properties in the chamber easier compared to the conventional techniques where only RF absorbers are used. The second technique targets to control shape of the Doppler spectrum in the chamber by controlling the angle of arrival (AOA). Conventionally, in the RVC, AOA is controlled by placing RF absorbers around the receiving terminal, which is described as effort consuming approach in [1] and its results are hard to reproduce. We show in this study that the effective way of controlling AOA and hence the shape of the Doppler spectrum is by placing absorbers around the source of mobility in the chamber (i.e stirrer in our case), and the logical behind this approach is explained. Significant novelties and contributions of this study can be listed as follows:

- The proposed channel emulation technique introduces degrees of freedom on controlling PDP of the channel emulated in the chamber. The necessity of using RF absorbers to control MPCs and RMS delay spread is minimized.

- With the proposed technique, even a bench-top sized chamber can be used to emulate channels with larger delay spread properties.

- The concept of using continuously rotating stirrer to emulate Doppler environment in the RVC is revisited, and the relationship between the stirrer and the created Doppler spectrum is established.

Evaluation of the proposed design is presented with measurements and mathematical analysis. Mathematical relationship of the emulated RMS delay and delays introduced by SAW delay lines is derived. Assessment of the statistical

distribution of EM fields in the RVC is also done to portray the positive effect of the proposed emulation technique on the field statistics. Delay spread, Doppler spread and fading rate statistics of the emulated channel are evaluated, and the results are compared to the existing mathematical models and on-site measurement results available in the literature to confirm the validity of the proposed channel emulation technique.

The rest of the thesis is organized as follows: The model of the proposed channel emulator and its mathematical analysis is presented in details in section II. Established measurement system, procedures, and the performance analysis of the emulator are given in Section III. Finally, Section IV concludes the thesis.

# Chapter 2

# Multipath Wireless Channel

Physical objects like buildings, trees and terrain features in the environment in which communication takes place cause propagation effects such as reflections, diffractions, and scattering of the transmitted signal. Thus the signal is received as multiple copies which are distorted differently. This multipath propagation phenomenon causes fluctuation in the level of the received signal power due to the vectorial combination of differently phase-shifted MPCs arriving at the receiving terminal. Mathematical model of these effects can be given in baseband impulse response of the multipath wireless channel as

$$h(t,\tau) = \sum_{r=1}^{N} a_r(t)e^{j\theta_r(t)}\delta(\tau - \tau_r(t)), \tag{2.1}$$

where $N$ is the total number of resolvable MPCs, $a_r(t)$ and $\tau_r(t)$ is the amplitude and excess delay of $r^{th}$ component respectively. $\theta_r(t)$ represents a phase term of each tap delay. $\delta(\cdot)$ is the Dirac delta function that models the resolvable MPCs according to their excess delays.

Fig. 2.1 represents a typical wireless channel scenario with a base station in the left transmitting signal to the user equipment (mobile phone) surrounded by a number of local scatters. In the following subsections, we will summarize several important aspects of the multipath channel.
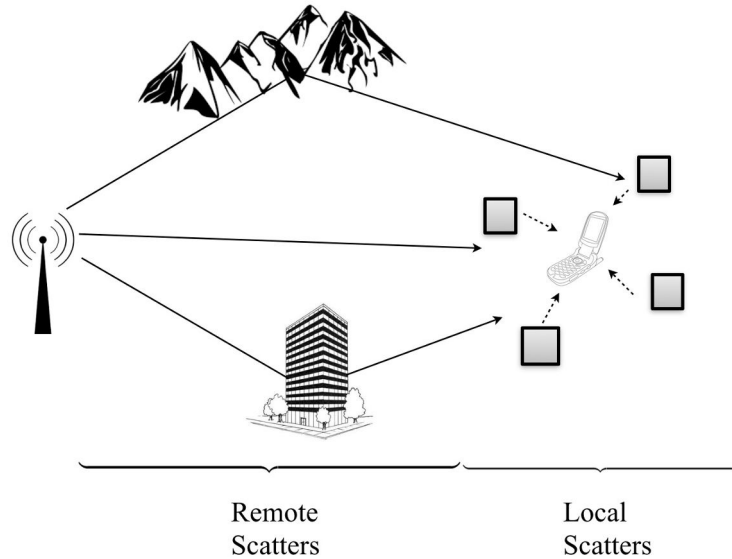
Figure 2.1: Typical wireless communication scenario

## 2.1 Local and Remote scatters

Local scatters, the scatters in the vicinity of the communication terminal give rise to the multipath signal components which are hard to isolate and thus they appear as a cluster or tap to the receiver. These unresolvable MPCs are the main cause of the Doppler spread and time selectivity of the channel in the presence of mobility. Multipath signal components reflected from remote scatters (i.e. high-rise buildings, mountains, etc.) experience significant delays of different degrees that cause the received signal to spread in time (time dispersion) [7,8].

In this study, the concept of local and remote scatters is imitated in the proposed channel emulation method to create a doubly dispersive channel inside RVC. Exploiting the ability of SAW delay lines to introduce large delays on the signal, we employ them to emulate the effect of the remote scatters whereas signal reflection within RVC emulates the effect of the scatters local to the receiver and the continuously rotating stirrer inside RVC serves as a source of mobility to emulate Doppler spread.

## 2.2 Time Dispersion

Random multiple reflections of the MPCs causes copies of the originally transmitted signal to arrive at the receiver at different instants leading to the spreading of the received signal in time-axis, the phenomenon termed as delay spread or time dispersion. Multipath channel metrics such as maximum excess delay $(\tau_{max})$, mean excess delay $(\tau_{mean})$, and RMS delay spread $(\tau_{rms})$ are commonly used to quantify time dispersion of the wireless channel. These metrics are derived from a PDP of the channel. PDP is presented as a plot of relative received power as a function of excess delay with respect to the first detectable signal arriving at the receiver. By averaging the power of each tap in time, PDP can be calculated as

$$PDP(\tau) = \langle | h(t, \tau) |^2 \rangle_t. \tag{2.2}$$

The RMS delay spread is the square root of the second central moment of the PDP and it can be calculated as

$$\tau_{rms} = \sqrt{\frac{\sum_{\tau}(\tau - \tau_{mean})^2 \cdot PDP(\tau)}{\sum_{\tau} PDP(\tau)}}, \tag{2.3}$$

where $\tau_{mean}$ is the mean excess delay of the channel. It is the first central moment of the PDP and can be calculated as

$$\tau_{mean} = \frac{\sum_{\tau} PDP(\tau) \cdot \tau}{\sum_{\tau} PDP(\tau)}. \tag{2.4}$$

Some important points to note about PDP are listed below:

- Typical shape of the PDP varies depending on the distribution of scatters in the radio propagation environment. For instance, maximum excess delay can vary from $0.5\mu s$ for rural areas to $20\mu s$ for mountainous environment [9]. Wittmann, et al. investigated the impact of the PDP shape on the bit error rate (BER) of the mobile radio system through computer simulation [10]. With the delay spread emulation technique introduced in this study, shape of the PDP obtained in RVC can be easily changed to match PDP shape of the desired scenario.

7

- Power delay profile represents power of the received communication signal as well as noise power associated with signal-to-noise ratio of that particular profile. Any component within noise floor is basically unwanted and should not be considered in the evaluation of delay spread as these components artificially lengthen the RMS delay [2, 11]. The convenient way of getting rid of noise effect in the RMS delay calculation is to set noise threshold on the PDP prior to calculation. Choice of the noise threshold modifies calculated value of RMS delay spread. To visualize effect of noise in the calculation of RMS delay spread equations (2.3) and (2.4) are re-written as follows [11]

$$\tau_{rms} = \sqrt{\frac{\sum_t (t - \bar{\tau}) \cdot [\widehat{PDP}(t) + n(t)]}{\sum_t [\widehat{PDP}(t) + n(t)]}}, \tag{2.5}$$

and

$$\bar{\tau} = \frac{\sum_t [\widehat{PDP}(t) + n(t)] \cdot t}{\sum_t [\widehat{PDP}(t) + n(t)]}, \tag{2.6}$$

where by $\widehat{PDP}$ represents theoretical PDP (noise free) and $n$ represent power of the noise samples.

## 2.3 Doppler Spread

The presence of mobility in the communication environment causes random frequency modulation due to different Doppler shifts on each of the MPCs. Each MPC is received with frequency $f'_c$ depending on the speed $V$ of the mobility and angle $\theta$ with which each component arrives/depart from the source of mobility in the scenario. This causes the received signal to spread in the frequency domain, a phenomenon referred to as Doppler spread or frequency dispersion. An expression for $f'_c$ is given by

$$f'_c = f_c + \frac{V}{\lambda} \cos \theta, \tag{2.7}$$

where $f_c$ is the actual carrier frequency of the system and $\lambda$ is the wavelength of the signal in the free space.

Two types of motion scenarios are discussed in the literature as the main sources of mobility in the communication scenarios; (i) relative motion between transmitter/receiver, (ii) motion of the surrounding objects in the communication scenario [1, 12]. The motion of the surrounding objects has been extensively adopted in the literature to emulate Doppler spread in the RVC by using continuously rotating stirrer. The rotational motion of the stirring paddles serves as a source of mobility in the RVC while the transmitting and receiving antennas are stationary [1, 13–15].

The speed of the mobility, operational frequency, motion intensity, and AOA are the factors evaluated in the literature to have a significant impact on the Doppler spread and shape of the Doppler spectrum. The relationship (2.7) tells that Doppler shift of each multipath component is directly proportional to the speed and operation frequency. By considering the scenario in which source of mobility is from the motion of the surrounding objects, only the MPCs that encounter the moving objects undergo Doppler effect while the rays that are reflected off the static objects in the surrounding do not. This introduces the concept of the motion intensity which refers to the ratio of the MPCs coming from stationary and moving objects [1, 16]. Thus, Doppler spread increases with the increase in the number of moving objects in the communication scenario.

## 2.4    Fading statistics

Fluctuation in the level of the received signal power due to the superposition of the MPCs at the receiver is termed as fading. Fading statistics of the channel is always of the great importance for deciding on the transmission parameters and coding schemes [17]. Quantitative description of the fading statistics is usually expressed in terms of level crossing rate ($LCR$) and the average fade duration ($AFD$). $LCR$ refers to the expected rate at which the received signal envelope crosses a specified level in a positive or negative-going direction [17] whereas $AFD$ defines the average time duration spent by the signal envelope below that level. Mobility in the communication scenario has strong impact on the fading rate of

the signal envelope [18], and it can be seen from its analytical expression given as

$$LCR(R) = \sqrt{2\pi} f_m \rho e^{-\rho^2}, \tag{2.8}$$

where $f_m$ is the speed of the mobile, and $\rho = R/R_{rms}$, with $R$ being the specified threshold level at which $LCR$ is observed. The study in [13] takes advantage of this relationship between $LCR$ and mobile speed to estimate maximum Doppler spread due to continuously rotating stirrer in the RVC. Other factors that have been studied in the literature to have a direct impact on the fading rate of the signal envelope includes richness of the MPCs due to scattering [19] investigated through simulation, and RMS delay spread of the channel [20] investigated analytically. In this study, the effect of RMS delay spread on the fading rate is practically investigated by using RVC.

# Chapter 3

# Proposed Channel Emulator

## 3.1 Overview Of Surface Acoustic Wave (SAW) Delay Lines

SAW devices convert electrical signal to acoustic (mechanical) wave which travels across its elastic surface (substrate) with much lower speed (approximately $10^5$ times lower) than its EM form [21]. Fig. 3.1(a) shows a structure of the SAW delay line, it consists of the piezoelectric substrate mounted with interdigital transducers (IDTs) on either side for the electrical-mechanical-electrical signal conversions. The gap between IDTs is known as microelectromechanical delay line through which an appreciable delay is introduced on the propagating signal.
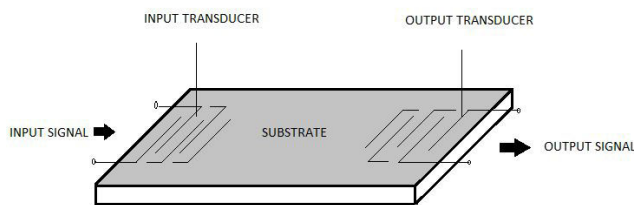


(a) SAW delay line Structure
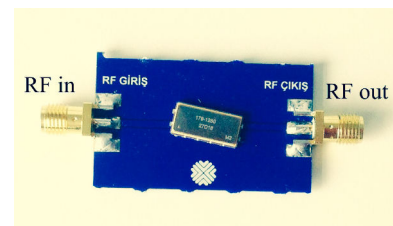
(b) Typical SAW delay line used in the measurement

Figure 3.1: SAW delay line

Some of the works in the literature that exploit the acoustic delay property of the SAW devices in various fields of communication include radar, satellite, and television systems, as well as signal processing applications, as outlined in [22]. In this study, SAW delay lines are employed as the key delay elements of the proposed wireless channel emulator as explained in the next subsection.

## 3.2    Proposed Channel Emulation Technique

Proposed channel emulator design utilizing SAW delay lines, RVC, power splitter, and power controllers is shown in Fig. 3.2. First, the input signal is divided into the desired number of paths by the splitter. Each path, representing tap in (2.1), is then passed through a particular SAW delay line depending on the amount of delay desired for it. Since the line of sight (LOS) is the first received channel tap, there is no delay line in the first path as it is designated to model the LOS path. However, if a propagation delay is desired to be introduced, all the path delays should be increased by the desired value, including the LOS path. Gain of each tap is adjusted by the power controllers to emulate $a_r(t)$ term in (2.1). From the power controllers, the signal is radiated into RVC to reverberate and consequently be captured by the receiving antenna.
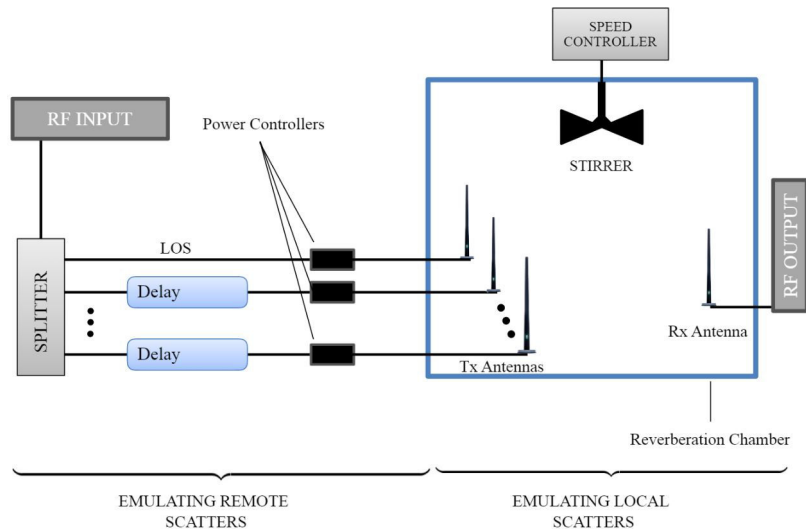


Figure 3.2: Block diagram of the proposed emulator

12

It is important to point out the following critical design factors about the proposed emulator:

- While the choice of splitter depends on the desired number of taps, a cascaded splitter network as shown in Fig. 4.2(b), can be used in the absence of the splitter with the desired number of outputs.

- It is known that while RF signal propagates through the air, it is attenuated due to pathloss. The longer the propagation distance the higher the pathloss. It is then important to incorporate the effect of the pathloss in our modeled signal taps. At this juncture, it is worth mentioning that SAW delay lines have insertion loss that attenuates signal passing through it. The amount of attenuation imposed on the signal varies from one model of SAW delay line to another. This inherent attenuation property of SAW devices can be considered as pathloss in realistic channel scenarios. Moreover, with the help of power controller (amplifiers/attenuators), this attenuation can still be adjusted to a desired value depending on the nature of the environment being emulated.

- Usage of continuously rotating stirrers with controllable speed in the RVC provides two important things, it provides field magnitude uniformity throughout the chamber as well as serves as a source of mobility and Doppler spread in RVC. By adjusting the speed of the stirrer, carrier frequency or controlling the angle of arrival of different MPCs, the amount of the Doppler spread induced into the signal as well as the shape of the Doppler spectrum can be controlled.

- Traditionally, the delay introduced by SAW device is independent of the operational frequency but it depends only on the acoustic surface wave velocity associated with the substrate material and the gap between the IDTs. However, since delay line are passive RF devices they are optimized to work for the specific frequency and specific delay. Thus changing delay value of a certain tap or operational frequency of the system involves changing the SAW delay line in the emulator.

Table 3.1 below highlights some advantages of the proposed emulator design over conventional RVC emulator.

Table 3.1: Proposed Emulator design versus conventional RVC emulator

| | Proposed Emulator | Conventional RVC |
|---|---|---|
| Delay spread control | Chamber size is not a limiting factor:<br><br>• High RMS delay can be achieved even with small chambers.<br><br>• RMS delay can be reduced by reducing power of the taps with power controllers. | Limited by Chamber size:<br><br>• High RMS delay can be achieved only with larger chamber.<br><br>• Small RMS delays can be achieved by RF absorbers loading only which disturbs statistical properties of the EM field inside RVC. |
| PDP shape | Configurable profiles:<br><br>• PDP with multiple discrete clusters can be achieved (like PDP observed in urban and mountainous scenarios). | Achieves PDP with constant shape<br><br>• Exponentially decaying PDP. |
| Shape of the Doppler spectrum | Achieves better control of the Doppler spectrum shape by placing absorbers around the source of mobility. | Doppler spectrum shape is manipulated by placing absorbers around receiving terminal |

## 3.3   Analysis of the emulated delay spread

Delay spread characteristics of the proposed emulator is analyzed by using the PDP and time dispersion metrics (i.e. maximum excess delay ($\tau_{max}$), mean excess delay ($\tau_{mean}$), and RMS delay spread ($\tau_{rms}$)) of the emulated channel. In [23], it is already confirmed theoretically that PDP of the mode stirred RVC obeys an exponentially decaying function with time constant $\tau_c = Q/\omega$, where $Q$ is the

quality factor of the RVC, and $\omega$ is the operational angular frequency ($\omega = 2\pi f_c$, with $f_c$ being the carrier frequency). Therefore, PDP for the plain RVC can be given as,

$$PDP(\tau) = P_o e^{-\frac{\tau}{\tau_c}} = P_o e^{-\frac{\omega}{Q}\tau}, \tag{3.1}$$

where $P_o$ is the tap's maximum power. If more taps are introduced by using SAW delay lines as it is designed in fig. 3.2, the equation (3.1) can be re-written as

$$PDP(\tau) = \sum_{n=0}^{N-1} P_n e^{-\frac{\omega}{Q}(\tau - \tau_{SAW_n})} \cdot u(\tau - \tau_{SAW_n}), \tag{3.2}$$

where $N$ is the number of the created taps, $\tau_{SAW_n}$ is the delay of the SAW delay line used to create the $n^{th}$ tap, and $u(\cdot)$ is the unit function. Note that, the case with $n = 0$ models LOS tap with its $\tau_{SAW_0} = 0$. The RMS delay spread of the emulated channel is then calculated as the second central moment of this PDP, given by

$$\tau_{rms} = \sqrt{E\{\tau^2\} - \tau_{mean}^2}, \tag{3.3}$$

where $E(\cdot)$ is the expectation, $\tau_{mean}$ is the mean excess delay of the channel calculated as the first central moment of the PDP as follows:

$$\tau_{mean} = \frac{\int_0^\infty \tau PDP(\tau)\,d\tau}{\int_0^\infty PDP(\tau)\,d\tau} = \frac{\sum_{n=0}^{N-1}\left(\int_{\tau_{SAW_n}}^{a} \tau P_n e^{-\frac{\omega}{Q}(\tau - \tau_{SAW_n})}\,d\tau\right)}{\sum_{n=0}^{N-1}\left(\int_{\tau_{SAW_n}}^{a} P_n e^{-\frac{\omega}{Q}(\tau - \tau_{SAW_n})}\,d\tau\right)}, \tag{3.4}$$

and

$$E\{\tau^2\} = \frac{\int_0^\infty \tau^2 PDP(\tau)\,d\tau}{\int_0^\infty PDP(\tau)\,d\tau} = \frac{\sum_{n=0}^{N-1}\left(\int_{\tau_{SAW_n}}^{a} \tau^2 P_n e^{-\frac{\omega}{Q}(\tau - \tau_{SAW_n})}\,d\tau\right)}{\sum_{n=0}^{N-1}\left(\int_{\tau_{SAW_n}}^{a} P_n e^{-\frac{\omega}{Q}(\tau - \tau_{SAW_n})}\,d\tau\right)}. \tag{3.5}$$

Note that, in (3.4) and (3.5), the upper limit of integration is changed from $\infty$ to $a = \tau_{SAW_{N-1}} - Q\ln(\alpha)/\omega$, where $\alpha$ is the normalized power level (see Appendix 6.1) through which the integration is performed. The parameter $10\log(\alpha)$ is referred as the threshold for dispersion calculations [24].

In Appendix 6.2, it is shown that, with further simplification of (3.4), and (3.5), $\tau_{rms}$ is found as

$$\tau_{rms} = \frac{Q}{\omega} \cdot \sqrt{A - B^2}, \tag{3.6}$$

15

where

$$\small A = \frac{\displaystyle\sum_{n=0}^{N-1} P_n \left[ \alpha \frac{\beta_{N-1}}{\beta_n} \left[ 2 \Big( \ln\alpha + \ln\beta_{N-1} - 1 \Big) - \Big( \ln\alpha + \ln\beta_{N-1} \Big)^2 \right] + \Big( \ln\beta_n - 1 \Big)^2 + 1 \right]}{\displaystyle\sum_{n=0}^{N-1} P_n \left( 1 - \alpha \frac{\beta_{N-1}}{\beta_n} \right)}, \tag{3.7}$$

$$\small B = \frac{\displaystyle\sum_{n=0}^{N-1} P_n \left( 1 - \ln\beta_n + \alpha \frac{\beta_{N-1}}{\beta_n} \Big( \ln\alpha + \ln\beta_{N-1} - 1 \Big) \right)}{\displaystyle\sum_{n=0}^{N-1} P_n \left( 1 - \alpha \frac{\beta_{N-1}}{\beta_n} \right)}, \tag{3.8}$$

and

$$\beta_n = \mathrm{e}^{-\frac{\omega}{Q}\tau_{SAW_n}}. \tag{3.9}$$

If we consider the conventional RVC where only LOS tap exists (i.e. $P_n = 0$, $\forall\, n \neq 0$, and $\tau_{SAW_0} = 0 \rightarrow \beta_0 = 1$), the $\tau_{rms}$ simplifies to

$$\tau_{rms} = \frac{Q}{\omega}\sqrt{\frac{\left[ (2\alpha\ln\alpha - 2\alpha + 2 - \alpha(\ln\alpha)^2) \right]}{(1-\alpha)} - \frac{\left[ 1 + \alpha(\ln\alpha - 1) \right]^2}{(1-\alpha)^2}}, \tag{3.10}$$

as established by Van't Hof in [24]. For an ideal RVC, $\alpha \rightarrow 0$, and (3.10) simplifies to $\tau_{rms} = Q\big/\omega$ which is the RMS delay spread of an ideal PDP.

For the conventional RVC whose $\tau_{rms}$ is given by (3.10), only Q-factor and operational frequency, $\omega$ can be adjusted to control delay spread. On the other hand, with the proposed channel emulation technique, powers $P_n$, and delays $\tau_{SAW_n}$ of the created taps are added as new degrees of freedom for controlling $\tau_{rms}$ of the channel emulated in the chamber as it can be deduced from (3.6) - (3.9).

## 3.4 Emulation of Doppler spread

Continuously moving stirrer with fixed receiver/transmitter configuration is one way of emulating Doppler spread inside RVC. Considering the rotational motion of the stirrer, different parts of the stirring paddles experience different effective linear speed $V$ depending on the distance $r$ from the axis of rotation and angular speed $\omega_p$ of the stirrer as illustrated in Fig. 3.3. Consequently, Doppler effect experienced by the MPCs in the RVC is also a function of $r$. With that being said, (2.7) is rewritten as,
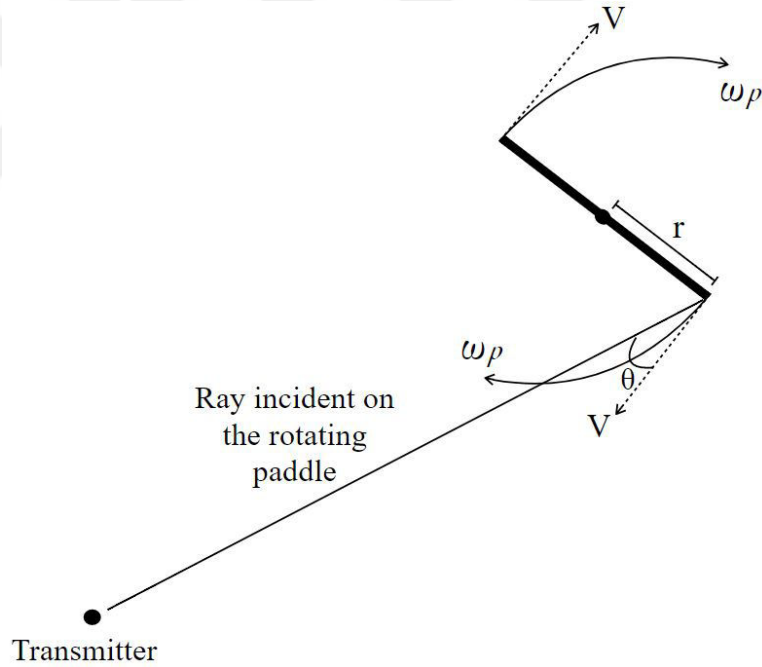


Figure 3.3: Stirrer as a source of Doppler spread

$$f_c' = f_c + \frac{\omega_p \cdot r}{\lambda} \cos \theta. \tag{3.11}$$

The presence of $r$ in (3.11) suggests that size of the stirrer has an impact on the amount of Doppler spread induced into the signal. With all other factors kept constant, stirrer with larger paddle size causes larger Doppler spread. Each of the factors affecting Doppler spread as mentioned in Section 2.4 can be emulated in the RVC by introducing different stimuli conditions as outlined in Table 3.2

17

below.

Table 3.2: RVC stimulus for Doppler spread emulation.

| Factor | RVC Stimulus |
|---|---|
| Speed of Mobility | Speed of the Stirrer |
| Operational Frequency | Operational frequency in RVC |
| Motion Intensity | Number of stirrers in the RVC |
| Angle of arrival | Position of RF absorbers around the stirrer |

Effect of AOA (i.e. $\theta$ in (3.11)) on the shape of the Doppler spectrum is investigated by using RF absorbers. On the scenario presented by Fig 3.3, the two sides of the stirrer have the same but opposite effective linear speed $V$, which causes negative and positive Doppler shifts of the incident rays from the transmitter. This suggests that the meaningful and effective way of controlling the resultant shape of the Doppler spectrum is by placing RF absorbers around the stirrer itself. Placing the absorbers on other parts of the RVC or around receiving antenna only causes non-isotropic reception of the signal with an insignificant effect on the Doppler power spectrum.

# Chapter 4

# Measurements and Performance Analysis

In the measurement and testing phase, the emulator design shown in Fig. 3.2 was evaluated in 5G and Beyond Research laboratory at Istanbul Medipol University. The proposed design was implemented using the following components:

- Reverberation chamber with the dimensions of 68 $cm$ x 120 $cm$ x 55 $cm$

- Fan (as a stirrer) from FanexFan Technology, with controllable speed and paddle radius of 0.15 $m$.

- RF absorbers

- A179-1250M2 SAW delay line with:

  - 1.25 $GHz$ center frequency

  - 530 $MHz$ bandwidth

  - 660 $ns$ delay

  - 29 dB insertion loss (attenuation)

- A179-1250M3 SAW delay line with:

– 1.25 $GHz$ center frequency

– 530 $MHz$ bandwidth

– 306 $ns$ delay

– 29 dB insertion loss (attenuation)

- Mini-Circuit ZN2PD2-63-s+ power splitters/combiners

- Mini-Circuit Coaxial SMA fixed attenuators

- VERT 900 Ettus omnidirectional antennas

While Fig. 4.1 shows the block diagrams of the measurement setups used in our experiments, Fig. 4.2 shows the actual RVC used in our measurement and cascaded splitter network used to create three taps channel in RVC. For the detailed evaluation of the time spread characteristics of the proposed emulator, four measurement scenarios were considered as summarized in Table 4.1. Scenario 1 is a plain RVC, used to compare our results with the conventionally implemented RVC channel emulators. Scenario 2 and 3 emulate 2 tap channel with different maximum excess delays, whereas scenario 4 emulates 3 tap channel. With these scenarios, the achieved maximum excess delay and the RMS delay spread are investigated to determine their relation to the delay introduced by the delay lines.



(a) VNA measurement setup

(b) Doppler Measurement Setup with absorbers in one side of the stirrer
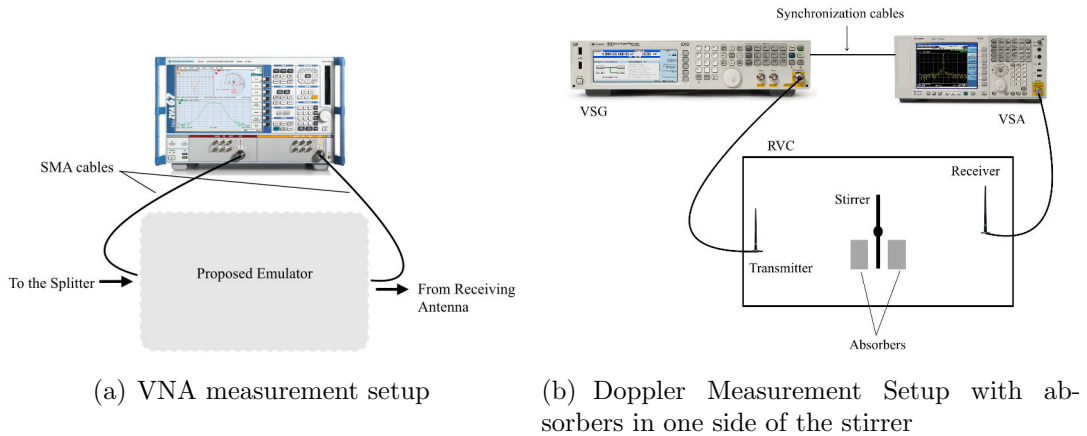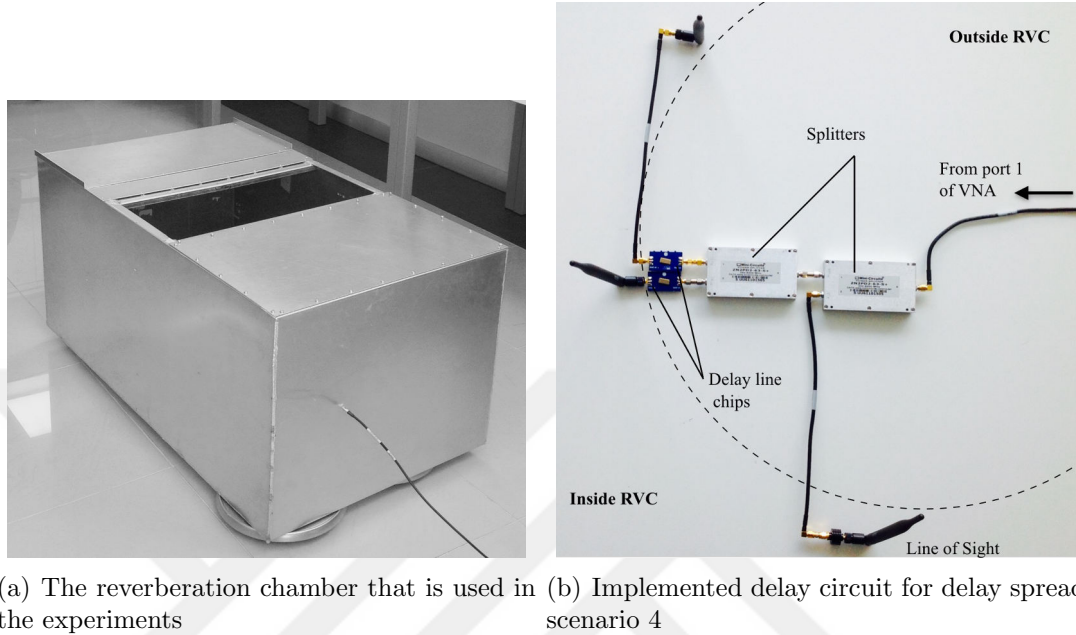
Figure 4.1: Measurement setups

(a) The reverberation chamber that is used in the experiments

(b) Implemented delay circuit for delay spread scenario 4

Figure 4.2: Other Measurement equipments

As we have mentioned in section 3.4, our approach to investigate the impact of AOA on Doppler spectrum involves controlling angular spread around the stirrer (the source of mobility). To introduce differences in the angular spread, the RF absorbers were used to block some MPCs arriving at the stirrer from a particular direction as shown in Fig. 4.1(b). Three scenarios are considered for the Doppler spectrum shape investigation as outlined in the second column of Table 4.1. The 'No absorber' case in scenario 1 gives a standard Doppler spectrum for comparison purpose with scenarios 2, and 3.

## 4.1   Channel Statistics Analysis

Performance of RVC in the wireless channel emulation and in other EM field measurement applications relies much on how well its working space[1] is spatially uniform which ensures that the measured samples are totally random and

---

[1]Working space of the RVC refers to the region in the RVC that is well stirred and thus EM field distribution in this region is considered to be statistically uniform.

Table 4.1: Measurement Scenarios

| Delay Spread | Doppler spread |
|---|---|
| Scenario 1:<br><br>• One tap - LOS.<br><br>• No delay line.<br><br>• Plain RVC | Scenario 1:<br><br>• No absorber. |
| Scenario 2:<br><br>• Two taps - LOS & S1 .<br><br>• Delay line with 306 $ns$ delay. | Scenario 2:<br><br>• Absorbers around one half of the stirrer. |
| Scenario 3:<br><br>• Two taps - LOS & S2 .<br><br>• Delay line with 660 $ns$ delay. | Scenario 3:<br><br>• Absorbers around the other half of the stirrer. |
| Scenario 4:<br><br>• Three taps - LOS, S1 & S2 .<br><br>• Delay lines with 306 $ns$ delay (S1) and 660 $ns$ delay (S2). | |

independent. The spatial uniformity can be achieved by using mode-stirring techniques such as frequency stirring, antenna position stirring (spatial stirring) and paddle position stirring while taking the measurements. Since the RVC used in this study is relatively small, the combination of all these stirring mechanisms was applied to ensure that the chamber is operating at high enough mode density as suggested in [25]. Assessment of the mode density was done by examining the frequency response of the emulated channel. Analytical and measurement analysis in [24] show that the frequency response of the undermoded working space is characterized by separated individual resonant peaks. Such peaks are not identifiable in the case of overmoded region due to the overlapping of many significant modes at any one of the given frequencies. Fig. 4.3 shows that, with

the combination of the stirring mechanisms, our RVC was excited with high number of modes. The frequency response used to plot fig. 4.3 was obtained through channel sounding by using VNA and conventional RVC setup.
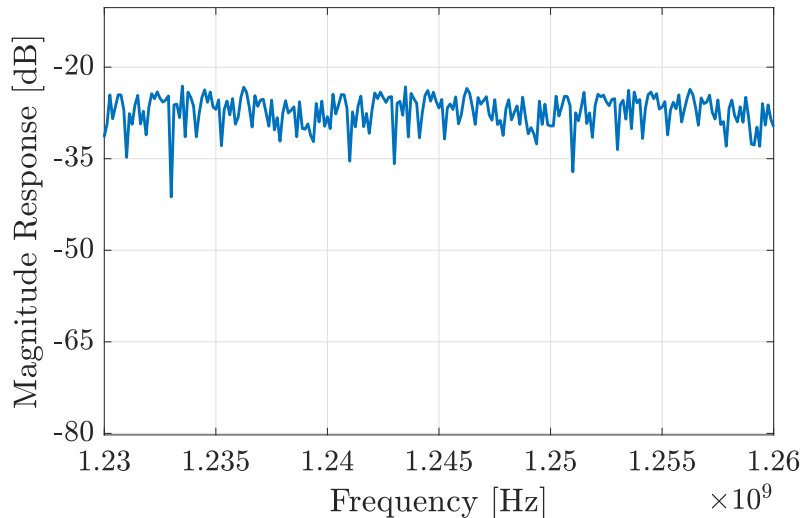


Figure 4.3: Magnitude of the frequency response (S21-parameter) displaying no identifiable individual resonant peaks. For better visualization, only a portion of the operational bandwidth is displayed.

Using the VNA setup given in fig. 4.1(a), 4001 frequency points were swept for each of 10 different paddle positions and 5 spatial positions, making up a total of 200050 measurement samples collection for each scenario for probability density function (PDF) estimation. Paddle-position stirring was achieved by using approach discussed in [26], but with larger step size (about 36°) to ensure uncorrelated paddle positions. Fan was operated at low speed (1 revolution for 30s) in order to have a slow time-varying channel in the chamber. This is to allow enough time for VNA frequency-sweeping to take place [12]. Measurement were recorded after every 3s, making the total measurement time of 30s at each spatial position. Spatial-stirring was done by moving the receiving antenna to 5 different locations within RVC while keeping the rest of the measurement setup the same.

Spatial uniformity of the EM field in the RVC was evaluated in two ways. First, by plotting distribution of the measured data and compare them with the PDF predicted for an ideal chamber (Rayleigh PDF) for the scenarios with and without SAW delay lines. Second, by calculating and comparing standard deviations of the measured samples in each of these scenarios. In this context, we investigated the impact of using SAW delay lines on the field uniformity in the RVC.
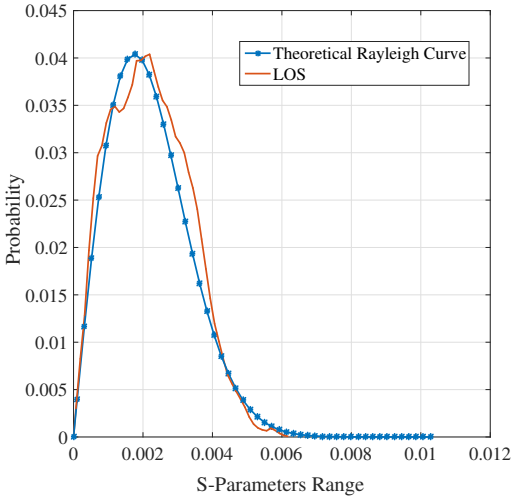


(a) one tap: LOS
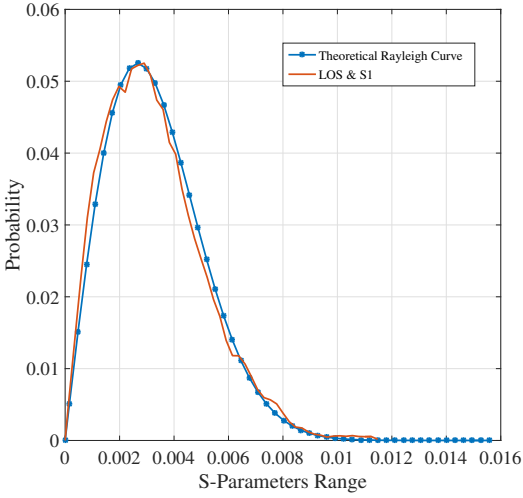


(b) Two taps: LOS and S1
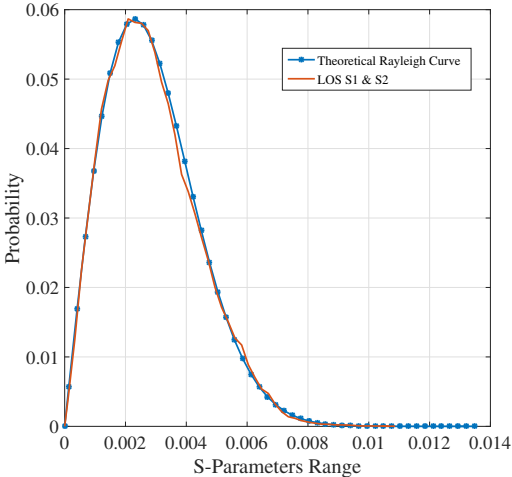


(c) Three taps: LOS S1 and S2

Figure 4.4: Statistical distributions for different number of taps featuring SAW delay lines

Fig. 4.4 presents statistical distribution (PDF) of the amplitudes of the captured signal for scenarios with the different number of taps. As the number of taps increases, statistics of the respective scenario better fits to the theoretical Rayleigh distribution. This depicts the fact that spatial uniformity of the field created within RVC gets improved. It is obvious that superposition of the EM fields simultaneously generated by more than one antenna improves spatial uniformity [27], but the concern here is to show that presence of SAW delay lines would not break this custom and thus it is safe to use them without worrying about any field uniformity distortion in the chamber. The same conclusion can be derived by observing the variation of standard deviations of field distribution within RVC as shown in Table 4.2.

Table 4.2: Variation of Standard Deviation with increasing number of taps in RVC.

| Num. Taps | Tap | Standard Deviation (dB) |
|-----------|-----------|-------------------------|
| 1 | LOS | 26.05 |
| 2 | LOS S1 | 23.78 |
| 3 | LOS S1 S2 | 20.24 |

Table 4.2 presents values of the standard deviations of field distribution within RVC as calculated for the different number of taps. As it could be expected, standard deviation decreases with the increase in the number of taps. This trend is not surprising as it completely abides with results presented in [27] and agrees with implication that can be drawn from [2], regardless the incorporation of SAW delay lines in our setup. The decrease in standard deviation values implies the improvement of spatial uniformity of the EM field inside RVC.

## 4.2   Enhanced delay spread in RVC

Rohde Schwarz ZVA67 Vector Network Analyzer (VNA) was used in the measurements to evaluate the proposed channel emulator with the measurement setup shown in Fig. 4.1(a). The VNA sweeps the channel over a specified frequency

band by stepping through discrete frequencies. Thus, the frequency response of the channel is obtained as the scattering parameters (S-parameters). By taking the inverse discrete Fourier transform ($IDFT$) of the measured frequency response, $H(f)$, the time domain channel impulse response (CIR), $\hat{h}(t,\tau)$, for the measurement instant can be calculated as,

$$\hat{h}(t,\tau) = IDFT\{H(f)\}. \tag{4.1}$$

The PDP of this discretely measured CIR is found by using equation 2.2 and its RMS delay spread is calculated by 2.3

The VNA was set to sweep 500 $MHz$ span (1000 $MHz$ - 1500 $MHz$) and calibrated by following its guideline. The frequency range was selected to not exceed the operational bandwidth of the delay lines. 4001 frequency samples with the resolution bandwidth of 125 $kHz$, were observed and transferred to MATLAB to determine PDP, and $\tau_{rms}$ of the measured channel.

Table 4.3: Relationship between RVCs maximum excess delay spread and delay of the SAW delay line.

| Scenario | Chip of the highest delay ($\tau_{SAW_{max}}$) | Achieved maximum excess delay ($\tau_{max}$) ($ns$) |
|---|---|---|
| LOS | None | $392 = 0 + 392$ |
| LOS S1 | S1 $= 306\ ns$ | $670 = 306 + 364$ |
| LOS S2 | S2 $= 660\ ns$ | $1000 = 660 + 340$ |
| LOS S1 S2 | S2 $= 660\ ns$ | $1022 = 660 + 362$ |

As explained in Section 2.2, we have considered setting a noise threshold before evaluating the delay spread characteristics of the measured signal. With noise threshold at 30 $dB$ below the maximum normalized power, RMS and maximum excess delays achieved with the plain RVC (LOS scenario) was 54 $ns$ and 392 $ns$ respectively (Fig. 4.5(a)). Incorporation of SAW delay lines with RVC enhanced the achieved delay spread values of the chamber as observed in Fig. 4.5(b)-4.5(d). The increase in the maximum excess delay was found to depend on the chip of the highest delay used in the particular scenario as analyzed in Table 4.3. The last column of Table 4.3 reveals that the maximum excess delay ($\tau_{max}$) achieved in each scenario is approximately equal to the sum of the delay of the highest
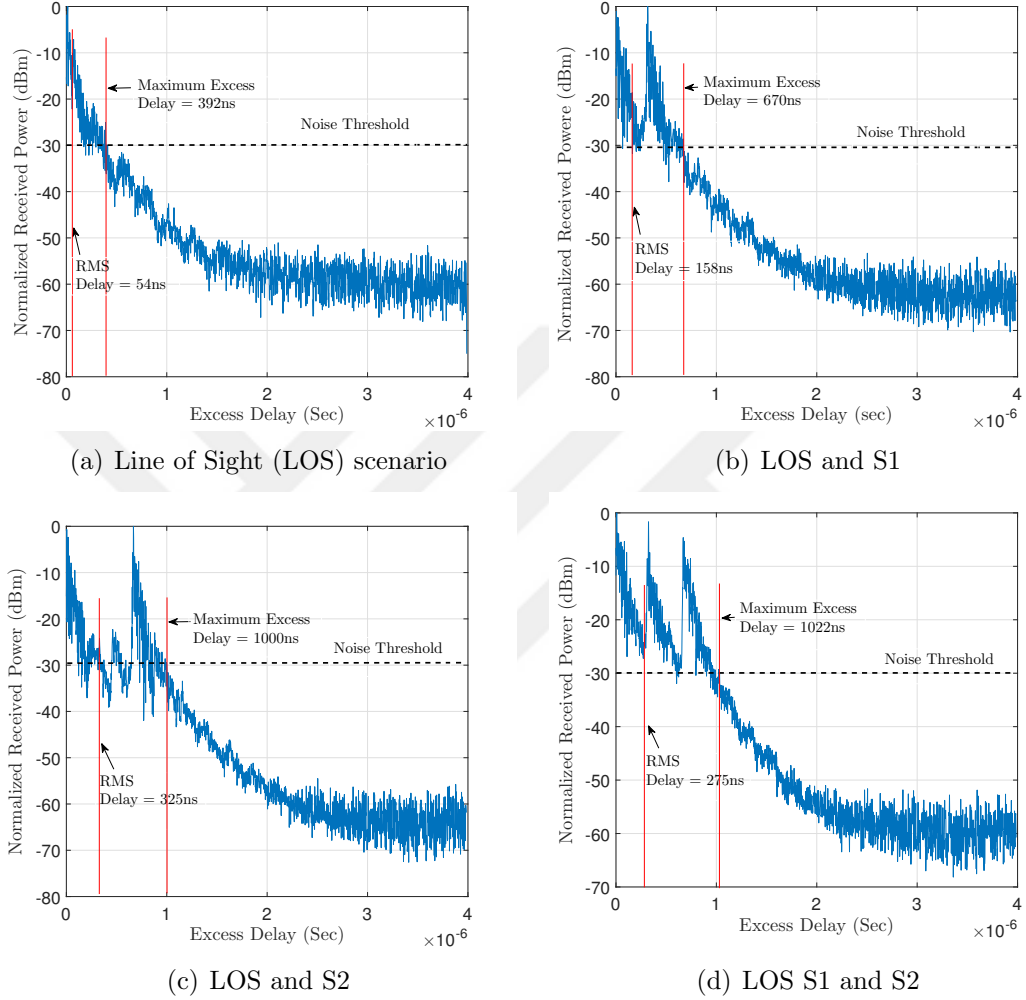
(a) Line of Sight (LOS) scenario      (b) LOS and S1

(c) LOS and S2           (d) LOS S1 and S2

Figure 4.5: Power delay profiles for scenarios with different number of taps in RVC

delay line ($\tau_{SAW_{max}}$) in that particular scenario and the maximum excess delay of the plain RVC with some fluctuations due to noise. This relationship can be summarized as,

$$\tau_{max} = \tau_{max_{RVC}} + \tau_{SAW_{max}}, \tag{4.2}$$

where $\tau_{max_{RVC}}$ is the maximum excess delay that can be achieved with the plain RVC. Therefore, with the knowledge of $\tau_{max_{RVC}}$, proper choice of SAW delay line can be made according to (4.2) and the desired higher maximum excess delay ($\tau_{max}$) can be achieved even with small-sized RVC. This can also be very helpful when testing communication systems which are sensitive to the maximum

27

excess delay spread of the channel such as OFDM (Orthogonal frequency division multiplexing) based systems, for instance, cyclic prefix, (CP), size of OFDM symbol is chosen according to maximum excess delay of the channel so as to mitigate the effect of the Inter symbol interference (ISI).

Table 4.4: Relationship between RMS and LOS power.

| LOS Attenuation (dB) | RMS delay spread ($\mu$sec) |
|---|---|
| 0 | 0.059 |
| 20 | 0.121 |
| 30 | 0.226 |
| 40 | 0.299 |

Table 4.4 shows the trend of RMS delay due to the decreasing power of LOS tap. In this case power of LOS path was decreased gradually by using attenuators to observe its effect on RMS delay spread. RMS excess delay was found to increase with the decrease in LOS power, in other words, RMS delay becomes larger as approaching a non line of sight (NLOS) scenario. This observation is well supported by the results obtained in measurement campaign conducted in [28] and [29], i.e. the NLOS scenarios were observed to exhibit higher RMS delay spread compared to the LOS scenarios.

## 4.3   Fading Rate Statistics

Measurements for fading statistics can be done in two ways depending on whether the fading analysis is done in time or frequency domain. $LCR$ and $AFD$ discussed in Section 2.4 are defined for time domain received signal envelope. VNA setup presented by Fig. 5(a), with VNA settings switched to the continuous wave mode (CW-mode), can be used to capture a complex time signal for the time domain fading rate investigation [30].

The study in [20] introduces the way of analyzing the fading statistics of the channel in frequency domain whereby fading rate is calculated from the frequency

domain signal envelope $E(f)$. We have adopted this approach in our measurements. We obtained $E(f) = |H(f)|$ where by $H(f)$ is the channel frequency response as obtained in Section 4.2. Consequently, $LCR_f$ is redefined as an average number of crossings per hertz bandwidth at which $E(f)$ crosses a level $R$ in the positive or negative going direction. The counterpart of $AFD$ is also defined as the average bandwidth of fade ($ABF$), which is the average amount of the bandwidth over which $E(f)$ is below $R$.
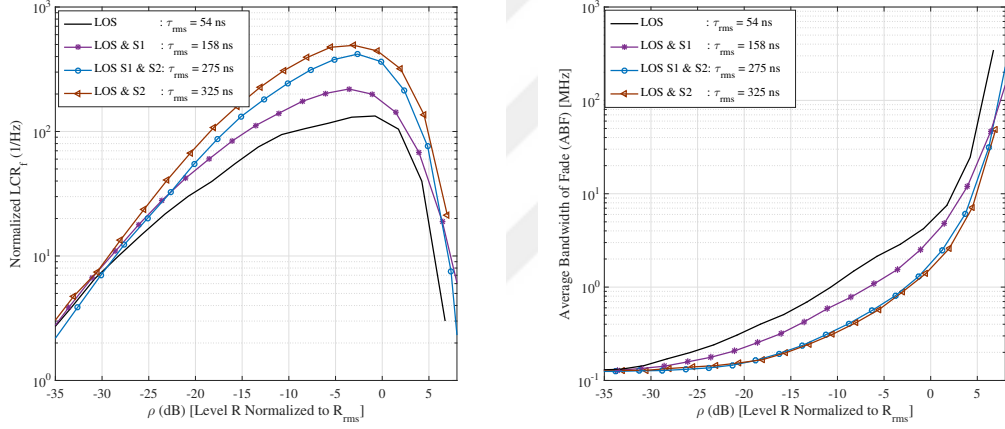


(a) $LCR_f$ measured for different RMS delay spread scenario

(b) ABF measured for different RMS delay spread scenario

Figure 4.6: Fading statistics

Shown in Fig. 4.6 are curves for the measured $LCR_f$ and $ABF$ for scenarios with different $\tau_{rms}$. Trend of the curves in Fig. 4.6(a) depicts that $LCR_f$ increases with the increase in $\tau_{rms}$ of the channel. This observation is in good accordance with the analytical relationship

$$LCR_f(R) \cong 2\sqrt{\pi}Re^{-R^2}\tau_{rms}, \qquad (4.3)$$

developed in [31], where $R$ is the threshold level at which $LCR_f$ is observed. (4.3) shows that, for Rayleigh channels, $LCR$ in the frequency domain is directly proportional to $\tau_{rms}$. Considering the relationship between $LCR_f$ and $ABF$ given in [20], which is

$$ABF(R) = \frac{P(R)}{LCR_f(R)}, \qquad (4.4)$$

with $P(R)$ being the probability that the envelope $E(f)$ is below level $R$ (i.e. $P(R) = P\{E(f) \leq R\}$), it can be easily deduced that,

$$ABF(R) \propto \frac{1}{\tau_{rms}}, \tag{4.5}$$

which is basically the conclusion that can be drawn from Fig. 4.6(b). The higher the $\tau_{rms}$ the shorter the signal envelope dwells below level $R$.

## 4.4   AOA and Doppler Spread

Keysight Technologies N5172B Vector Signal Generator (VSG) and N9010A Vector Signal Analyzer (VSA) devices were employed for the Doppler spread measurements with the setup shown in Fig. 4.1(b). VSG-VSA pair was time and frequency synchronized via cables from their respective synchronization ports. During the measurements, the fan was operated at a fixed speed of 11 $rps$ which corresponds to the maximum linear speed of 10.4 $m/s$. This speed is expected to cause the maximum Doppler shift ($f_{shift_{max}} = (V \cdot f_c)/c$) of about 43.3 $Hz$ whenever the MPCs interact with the fan, where $f_c = 1.25GHz$ is the carrier frequency, and $c = 3x10^8$ $m/s$ is the speed of light. However, it should be understood that, due to the resonant nature of RVCs, the effective Doppler spread in the RVC is usually larger than its theoretically calculated value [14].

A tone generated by VSG was sent at 1250 $MHz$ as an input to the RVC. Received signal was recorded for 30 $sec$ by the VSA. During all Doppler measurements, span of the VSA was set to 1 $kHz$ that corresponds to the sampling rate ($f_s$) of 1.28 $kHz$ in accordance to the data sheet of the used VSA model (i.e $f_s = Span * 1.28$. The fan was operated at 11 $rps$ which corresponds to the maximum linear speed of 10.4 $m/s$. The captured signal was processed in MATLAB software for further analysis. Doppler spreading was revealed by plotting power spectral density (PSD) of the received signal.

Fig. 4.7(a) shows the received tone that is spread in frequency due to the Doppler effects generated by the rotating stirrer in the RVC. Increasing resolution

(a) Received signal spreaded in frequency

(b) Received signal with high resolution to reveal individual Doppler shifted Multipath components
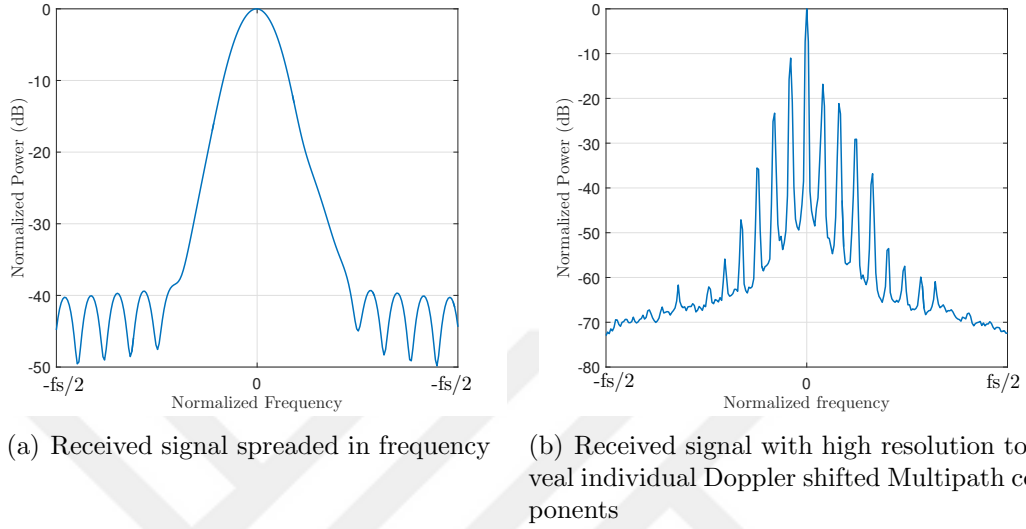
Figure 4.7: Doppler Spectrum of the received tone

of Fig. 4.7(a), MPCs with different amount of Doppler shifts are revealed as shown in Fig. 4.7(b). The finite number of MPCs observed in Fig. 4.7(b) tells that only those components that get in contact with the stirrer (source of mobility in the scenario) undergo Doppler shifts and thus contribute to the Doppler spectrum. Recalling the concept of motion intensity, more shifted components would be observed in Fig. 4.7(b) if more than one stirrers were placed in the RVC [1]. The observed Doppler spectrum exhibits a peak at the carrier frequency and the decay at the shifted components. This agrees well with analytical and measurements results presented in the literature [16, 32] for the similar scenarios (mobility due to surrounding objects) such as indoor communication. Furthermore, scattering effects of rotating helicopter blades and wind turbines can be evaluated to cause similar kind of Doppler spread like the one created by rotating fan in this study [Reference].

Fig. 4.8 shows the effect of placing RF absorbers around the stirrer to block some components from particular directions. Depending on the position of the absorbers, some of the MPCs are highly attenuated while others are maintained. Therefore, only MPCs arriving from a particular direction are affected by Doppler, resulting into the more asymmetric shape of Doppler spectrum. Although it is

31
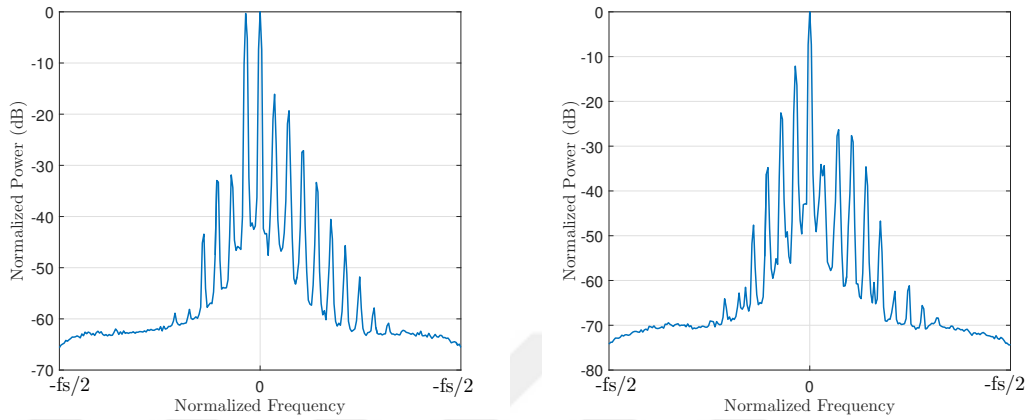
(a) RF absorbers in one side of the stirrer    (b) RF absorbers in the other side of the stirrer

Figure 4.8: Doppler Spectrum obtained with RF absorbers

difficult to predict the direction of arrival for each MPC (due to random multiple reflections inside RVC), the obtained results still give a good insight in understanding the relationship between AOA and Doppler spread phenomenon for better control of the Doppler spectral shapes.

# Chapter 5

# Conclusion

Although conventional RVC emulators provide an outstanding testbed for testing and evaluating the newly developed wireless systems, they are not flexible enough to emulate a wide range of wireless channel characteristics unless they are merged with other techniques to improve their capability. Conventional approaches focus more on improving emulation of a specific channel aspect at a time while ignoring the fact that any change (e.g. loading RF absorbers) in the RVC can simultaneously affect delay spread, Doppler spread and spatial uniformity of the EM field. In this study, a novel way of controlling MPCs inside RVC by using SAW delay lines and power controllers is proposed to reduce the required use of RF absorbers. The implemented channel emulator has provided great flexibility in manipulating delay and Doppler spread characteristics inside RVC. The proposed emulation technique not only grants full control of the emulated PDP shape but also enhances maximum achievable RMS delay spread introduced by the small-sized RVCs. However, limited applications of the SAW delay lines in the market poses some limitations on the operational frequencies and delay specifications. The proposed use of SAW delay lines in the channel emulators can provide new research areas for the field. Especially, delay lines with electronically controllable delays would provide an easier way of introducing different PDPs for the emulated channels which would remove the need for a new circuit for every new PDP.

# Chapter 6

# Appendix

## 6.1 Appendix A: Derivation of the Upper Limit of the Integration

Illustrated in fig. 6.1 is the perspective of the PDP that can be obtained by using the proposed emulation technique. The noise threshold is always considered for the calculation of the dispersion parameters of the PDP.
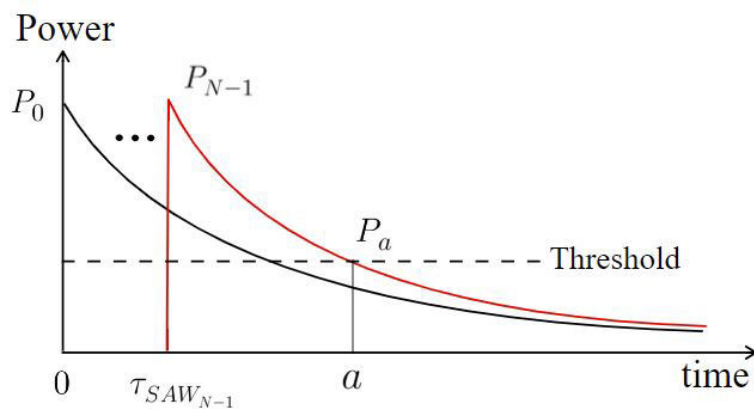


Figure 6.1: Typical PDP for the proposed emulation technique

The threshold power, $Pa$ in fig. 6.1 can be given as

$$P_a = Pe^{-\frac{\omega}{Q}(a - \tau_{SAW_{N-1}})}, \tag{6.1}$$

where $P$ is the composite power at time instant $\tau_{SAW_{N-1}}$, given by

$$P = P_0 e^{-\frac{\omega}{Q}(\tau_{SAW_{N-1}})} + \cdots + P_{N-1} = \sum_{n=0}^{N-1} P_n e^{-\frac{\omega}{Q}(\tau_{SAW_{N-1}} - \tau_{SAW_n})}. \tag{6.2}$$

Now, let $P_a/P = \alpha$, then, (6.1) becomes

$$\ln(\alpha) = -\frac{\omega}{Q}(a - \tau_{SAW_{N-1}}). \tag{6.3}$$

Consequently,

$$a = \tau_{SAW_{N-1}} - \frac{Q}{\omega} \ln(\alpha). \tag{6.4}$$

## 6.2 Appendix B: RMS Delay Spread of the Proposed Emulator

Here we will give the detailed derivation of the $\tau_{rms}$ expression given in (3.6) - (3.9) based on the discussion started in section ??. For notation simplicity, we abbreviate $\tau_{SAW_n}$ as $\tau_n$. First, let us simplify the numerator and denominator of (3.4) by using integration by parts technique as follows:

$$\int_{\tau_n}^{a} \tau P_n e^{-\frac{\omega}{Q}(\tau - \tau_n)} \, d\tau = P_n e^{\frac{\omega}{Q}\tau_n} \left[ -\frac{Q}{\omega} \tau e^{-\frac{\omega}{Q}\tau} - \left(\frac{Q}{\omega}\right)^2 e^{-\frac{\omega}{Q}\tau} \right]\Big|_{\tau_n}^{a}$$

$$= P_n e^{\frac{\omega}{Q}\tau_n} \left[ -\frac{Q}{\omega} a e^{-\frac{\omega}{Q}a} - \left(\frac{Q}{\omega}\right)^2 e^{-\frac{\omega}{Q}a} + \frac{Q}{\omega} \tau_n e^{-\frac{\omega}{Q}\tau_n} + \tag{6.5} \right.$$

$$\left. \left(\frac{Q}{\omega}\right)^2 e^{-\frac{\omega}{Q}\tau_n} \right].$$

By using (6.3), we can write

$$e^{-\frac{\omega}{Q}a} = \alpha e^{-\frac{\omega}{Q}\tau_{N-1}}. \tag{6.6}$$

Let

$$\beta_n = e^{-\frac{\omega}{Q}\tau_n}. \tag{6.7}$$

35

Now, by using (6.4), (6.6), and (6.7), (6.5) can be simplified into

$$\int_{\tau_n}^{a} \tau P_n e^{-\frac{\omega}{Q}(\tau-\tau_n)} \, d\tau = \left(\frac{Q}{\omega}\right)^2 P_n \left[1 - \ln\beta_n + \alpha\frac{\beta_{N-1}}{\beta_n}\left(\ln\alpha + \ln\beta_{N-1} - 1\right)\right]. \quad (6.8)$$

In the same manner, the denominator of (3.4) can be simplified as

$$\int_{\tau_n}^{a} P_n e^{-\frac{\omega}{Q}(\tau-\tau_n)} \, d\tau = P_n e^{\frac{\omega}{Q}\tau_n} \left[-\frac{Q}{\omega}e^{-\frac{\omega}{Q}\tau}\right]\Big|_{\tau_n}^{a} = \left(\frac{Q}{\omega}\right)P_n \left[1 - \alpha\frac{\beta_{N-1}}{\beta_n}\right]. \quad (6.9)$$

Substituting (6.8), and (6.9) into (3.4) we get

$$\tau_{mean} = \frac{Q}{\omega} \cdot \frac{\displaystyle\sum_{n=0}^{N-1} P_n \left(1 - \ln\beta_n + \alpha\frac{\beta_{N-1}}{\beta_n}\left(\ln\alpha + \ln\beta_{N-1} - 1\right)\right)}{\displaystyle\sum_{n=0}^{N-1} P_n \left(1 - \alpha\frac{\beta_{N-1}}{\beta_n}\right)}. \quad (6.10)$$

The same procedure can be applied to simplify (3.5) and get

$$\int_{\tau_n}^{a} \tau^2 P_n e^{-\frac{\omega}{Q}(\tau-\tau_n)} \, d\tau = P_n e^{\frac{\omega}{Q}\tau_n} \left[-\frac{Q}{\omega}\tau^2 e^{-\frac{\omega}{Q}\tau} - 2\left(\frac{Q}{\omega}\right)^2 \tau e^{-\frac{\omega}{Q}\tau} - 2\left(\frac{Q}{\omega}\right)^3 e^{-\frac{\omega}{Q}\tau}\right]\Big|_{\tau_n}^{a}$$

$$= \left(\frac{Q}{\omega}\right)^3 \cdot P_n \left[\alpha\frac{\beta_{N-1}}{\beta_n}\left[2\left(\ln\alpha + \ln\beta_{N-1} - 1\right) - \left(\ln\alpha + \ln\beta_{N-1}\right)^2\right] + \right.$$

$$\left.\left(\ln\beta_n - 1\right)^2 + 1\right].$$

$$(6.11)$$

Now, we use (6.9), and (6.11) to simplify (3.5) and obtain

$$E\{\tau^2\} = \left(\frac{Q}{\omega}\right)^2 \frac{\displaystyle\sum_{n=0}^{N-1} P_n \left[\alpha\frac{\beta_{N-1}}{\beta_n}\left[2\left(\ln\alpha + \ln\beta_{N-1} - 1\right) - \left(\ln\alpha + \ln\beta_{N-1}\right)^2\right] + \left(\ln\beta_n - 1\right)^2 + 1\right]}{\displaystyle\sum_{n=0}^{N-1} P_n \left(1 - \alpha\frac{\beta_{N-1}}{\beta_n}\right)}. \quad (6.12)$$

36

# Bibliography

[1] S. Güzelgöz, S. Yarkan, and H. Arslan, "Investigation of time selectivity of wireless channels through the use of RVC," *Elsevier J. Meas.*, vol. 43, no. 10, pp. 1532–1541, 2010.

[2] E. Genender, C. L. Holloway, K. A. Remley, J. M. Ladbury, G. Koepke, and H. Garbe, "Simulating the multipath channel with a reverberation chamber: Application to bit error rate measurements," *IEEE Trans. electromagn. compat.*, vol. 52, no. 4, pp. 766–777, 2010.

[3] C. L. Holloway, D. A. Hill, J. M. Ladbury, and G. Koepke, "Requirements for an effective reverberation chamber: Unloaded or loaded," *IEEE Trans. Electromagn. Compat.*, vol. 48, no. 1, pp. 187–194, 2006.

[4] P.-S. Kildal and C. Orlenius, "Characterization of mobile terminals in Rayleigh fading by using reverberation chamber," in *Proc. 18th Int. Conf. Appl. Electromagnetics Commun. (ICECom).*, (Dubrovnik, Croatia), pp. 1–4, IEEE, 2005.

[5] J. Frolik, T. M. Weller, S. DiStasi, and J. Cooper, "A compact reverberation chamber for hyper-Rayleigh channel emulation," *IEEE Trans. Antennas Propag.*, vol. 57, no. 12, pp. 3962–3968, 2009.

[6] J. F. Valenzuela-Valdés, A. M. Martínez-González, and D. A. Sánchez-Hernández, "Emulation of MIMO nonisotropic fading environments with reverberation chambers," *IEEE Antennas Wireless Propag. Lett.*, vol. 7, pp. 325–328, 2008.

[7] Paulraj *et al.*, *Introduction to space-time wireless communications*, ch. Space-Time propagation, pp. 11–31. Cambridge, United Kingdom: Cambridge university press, 2003.

[8] C. B. Paulraj, Arogyaswami J. Papadias, "Space-time processing for wireless communications," *IEEE Signal Process. Mag.*, vol. 14, no. 6, pp. 49–83, 1997.

[9] J.-P. De Weck, P. Merki, and R. W. Lorenz, "Power delay profiles measured in mountainous terrain (radiowave propagation)," in *Proc. Veh. Technol. Conf., 1988, IEEE 38th*, (Philadelphia, PA, USA), pp. 105–112, IEEE, 1988.

[10] M. Wittmann, J. Marti, and T. Kurner, "Impact of the power delay profile shape on the bit error rate in mobile radio systems," *IEEE Trans. Veh. Technol.*, vol. 46, no. 2, pp. 329–339, 1997.

[11] Z. Bodnar, Z. Herczku, and I. Frigyes, "Noise threshold dependency of the RMS delay spread in wideband measurements of radio propagation channels," in *Proc. SBT/IEEE Int. Telecommunications Symp. (ITS)*, (Sao Paulo, Brazil.), pp. 312–317, IEEE, 1998.

[12] T. S. Rappaport *et al.*, *Wireless communications: principles and practice*, vol. 2, ch. Mobile Radio Propagation: Small scale fading and multipath, pp. 139–196. Upper Saddle River, N.J: Prentice Hall PTR, 1996.

[13] X. Chen, P.-S. Kildal, and J. Carlsson, "Determination of maximum Doppler shift in reverberation chamber using level crossing rate," in *Proc. 5th European Conf. Antennas Propag. (EUCAP).*, pp. 62–65, IEEE, 2011.

[14] P. Hallbjorner and A. Rydberg, "Maximum Doppler frequency in reverberation chamber with continuously moving stirrer," in *Proc. Loughborough Antennas Propag. Conf. (LAPC).*, pp. 229–232, IEEE, 2007.

[15] K. Karlsson, X. Chen, J. Carlsson, and A. Skårbratt, "On OTA test in the presence of doppler spreads in a reverberation chamber," *IEEE Antennas Wireless Propag. Lett.*, vol. 12, pp. 886–889, 2013.

[16] S. Thoen, L. Van der Perre, and M. Engels, "Modeling the channel time-variance for fixed wireless communications," *IEEE Commun. lett.*, vol. 6, no. 8, pp. 331–333, 2002.

[17] J. D. Parsons, *The mobile radio propagation channel*, ch. characterization of multipath phenomena, pp. 114–162. West Sussex, England: Wiley, 2 ed., 2000.

[18] A. Sheikh, *Wireless communications: theory and techniques*, ch. Micro characterization of wireless channels, pp. 83–144. New York: Springer Science & Business Media, 2004.

[19] R. K. Ahmed, "Doppler fading communication channel performance simulation," *Int. J. Physical Sci.*, vol. 12, no. 7, pp. 89–94, 2017.

[20] K. Witrisal, Y.-H. Kim, and R. Prasad, "A new method to measure parameters of frequency-selective radio channels using power measurements," *IEEE Trans. Commun.*, vol. 49, no. 10, pp. 1788–1800, 2001.

[21] M. Hribšek, "Surface acoustic wave devices in communications," *Scientific Tech. Rev.*, vol. 58, no. 2, pp. 44–50, 2008.

[22] A. T. Alastalo, J. Kiihamäki, and H. Seppä, "Microelectromechanical delay lines with slow signal propagation," *IOP J. Micromech. Microeng.*, vol. 16, no. 9, p. 1854, 2006.

[23] D. A. Hill, M. T. Ma, A. R. Ondrejka, B. F. Riddle, M. Crawford, and R. T. Johnk, "Aperture excitation of electrically large, lossy cavities," *IEEE Trans. Electromagn. Compat.*, vol. 36, no. 3, pp. 169–178, 1994.

[24] J. P. Van't Hof, *Modeling the Dispersion and Gain of RF Wireless Channels inside Reverberent Enclosures*. PhD thesis, Carnegie Mellon Univ., Pittsburgh, PA., 2005.

[25] C. R. Dunlap, *Reverberation chamber characterization using enhanced backscatter coefficient measurements*. Ph.d thesis, Univ. Colorado, Boulder, CO, 2013.

[26] K. Karlsson, X. Chen, P.-S. Kildal, and J. Carlsson, "Doppler spread in reverberation chamber predicted from measurements during stationary stepwise stirring," *IEEE Antennas Wireless Propag. Lett.*, vol. 9, pp. 497–500, 2010.

[27] C. Yaozhong, W. Guanghui, F. Lisi, L. Xiaoqiang, and P. Xiaodong, "Effect of two emission antennas on field uniformity in a reverberation chamber," in *Proc. 2nd Int. Conf. Signal Process. Systems (ICSPS).*, vol. 3, (Dalian, China), pp. V3–227, IEEE, 2010.

[28] N. Moraitis, A. Kanatas, G. Pantos, and P. Constantinou, "Delay spread measurements and characterization in a special propagation environment for PCS microcells," in *Proc. 13th IEEE Int. Symp. Personal Indoor Mobile Radio Commun.*, vol. 3, (Pavilhao Altantico, Lisboa, Portugal.), pp. 1190–1194, IEEE, 2002.

[29] H. Shimizu, H. Masui, M. Ishii, K. Sakawa, and T. Kobayashi, "LOS and NLOS path-loss and delay characteristics at 3.35 GHz in a residential environment," *IEICE Trans. Fundamentals Electron. Commun. Comput. Sci.*, vol. 83, no. 7, pp. 1356–1364, 2000.

[30] A. Khaleghi, J.-C. Bolomey, and A. Azoulay, "On the statistics of reverberation chambers and applications for wireless antenna test," in *Proc. Int. Symp. Antennas Propag. Soc.*, pp. 3561–3564, IEEE, 2006.

[31] K. Witrisal, "On estimating the RMS delay spread from the frequency-domain level crossing rate," *IEEE Commun. Lett.*, vol. 5, no. 7, pp. 287–289, 2001.

[32] S. Howard and K. Pahlavan, "Doppler spread measurements of indoor radio channel," *Electron. Lett.*, vol. 26, no. 2, pp. 107–109, 1990.

# EMULATION TECHNIQUES FOR SMALL SCALE FADING ASPECTS OF WIRELESS CHANNEL BY USING REVERBERATION CHAMBER